Int. J. Heat Mass Transfer. Vol. 28, No. 5, pp. 909–918, 1985
Printed in Great Britain

0017 9310/85 $3.00 + 0.00

Heat and mass transfer by natural convection in a porous medium

ADRIAN BEJAN* and KHAIRY R. KHAIR
Department of Mechanical Engineering, University of Colorado, Campus Box 427, Boulder, CO 80309, U.S.A.

(*Received* 27 *April and in revised form* 30 *July* 1984)

Abstract—This paper reports a fundamental study of the phenomenon of natural convection heat and mass transfer near a vertical surface embedded in a fluid-saturated porous medium. The buoyancy effect is due to the variation of temperature and concentration across the boundary layer. The study contains two parts. In the first part, scale analysis shows that the natural convection phenomenon conforms to one of four possible regimes, depending on the values of buoyancy ratio N and Lewis number Le. The scales of the heat and mass transfer rates are determined for each regime. In the second part of the study, the boundary-layer problem is solved via similarity formulation in the buoyancy ratio range $-5 \leqslant N \leqslant 4$ and Lewis number range $1 \leqslant Le \leqslant 100$. The similarity solutions confirm the validity of the order-of-magnitude limiting results revealed by scale analysis.

1. INTRODUCTION

THE OBJECT of this work is to describe the most fundamental features of the natural convection boundary-layer flow driven by temperature and concentration variations near a vertical wall in a porous medium (Fig. 1). The novel aspect of this research is the focus on the often antagonistic relationship between the two buoyancy effects that drive the flow, namely, the density difference caused by temperature variations and the density difference caused by concentration variations. The engineering applications of this phenomenon are important; for example, the migration of moisture through the air contained in fibrous insulations and grain storage installations, and the dispersion of chemical contaminants through water-saturated soil. Despite these applications, and despite the strong interest expressed by the fluid mechanics community in the same phenomenon in fluids without a porous structure [1], the flow caused by competing buoyancy effects near a vertical wall in a porous medium remains to be investigated.

In the study of natural convection through porous media, the bulk of the research effort has been devoted to the flow caused by a single buoyancy effect, namely, the effect of temperature variations. The interest in this class of flows has been stimulated by heat transfer engineering applications such as geothermal energy conversion and thermal insulation design [2], hence, the two main configurations in which these heat transfer-driven flows have been studied are:

(i) porous layers heated from below;
(ii) porous layers heated from the side.

Relative to the research activity on Darcy flow driven by a single buoyancy effect, the work on convection driven by two buoyancy effects is quite limited, and, with very few exceptions, the work that has been published deals with configuration (i). The linear stability characteristics of the flow in horizontal layers with imposed vertical temperature and concentration gradients has been the subject of studies by Nield [3], Gershuni *et al.* [4] and Turner and Gustafson [5]. With regard to porous layers heated from the side, configuration (ii), the focus has been on the double-diffusive instability of the double boundary-layer structure that forms near a vertical wall immersed in a temperature and concentration stratified porous medium [6]. In a recent study, Raptis *et al.* [7] constructed similarity solutions for the boundary layer near a vertical wall immersed in a porous medium with constant temperature and concentration. Although this problem is related to the boundary-layer phenomenon addressed in the present study, it does not help in elucidating the fundamentals of configuration (ii), because it was based on the seemingly *ad hoc* assumption that the flow and all of its characteristics are independent of altitude.

2. MATHEMATICAL FORMULATION

Consider the boundary-layer flow near a vertical impermeable surface embedded in a porous medium saturated with fluid (Fig. 1). The surface is maintained at a constant temperature T_0 different than the porous medium temperature T_∞ sufficiently far from the wall. In addition, the concentration of a certain constituent in the solution that saturates the porous medium varies from C_0 on the fluid side of the vertical surface ($x = 0^+$) to C_∞ sufficiently far from the surface.

The equations governing the steady-state conservation of mass, momentum, energy and constituent for Darcy flow through a porous medium are [2]

$$\frac{\partial u}{\partial x} + \frac{\partial v}{\partial y} = 0 \tag{1}$$

$$u = -\frac{K}{\mu}\frac{\partial P}{\partial x} \tag{2}$$

* Current address: Department of Mechanical Engineering and Materials Science, Duke University, Durham, NC 27706, U.S.A.

NOMENCLATURE

c	similarity concentration profile
C	concentration
D	mass diffusivity
f	similarity streamfunction profile
g	gravitational acceleration
H	wall height
K	permeability
Le	Lewis number, α/D
N	buoyancy ratio, equation (38)
Nu	Nusselt number, equation (22)
P	pressure
Ra	Rayleigh number, equation (21)
Sh	Sherwood number, equation (24)
T	temperature
u, v	velocity components, Fig. 1
x, y	Cartesian coordinates, Fig. 1.

Greek symbols

α	thermal diffusivity
β	coefficient of thermal expansion
β_C	coefficient of concentration expansion
δ	velocity boundary-layer thickness, Fig. 2
δ_C	concentration boundary-layer thickness, Fig. 1
δ_T	thermal boundary-layer thickness, Fig. 1
ΔC	concentration difference, $C_0 - C_\infty$
ΔT	temperature difference, $T_0 - T_\infty$
η	similarity variable
θ	similarity temperature profile
μ	viscosity
ν	kinematic viscosity
ψ	streamfunction.

Subscripts

y	local property
0	wall property
∞	porous reservoir property.

$$v = -\frac{K}{\mu}\left(\frac{\partial P}{\partial y} + \rho g\right) \tag{3}$$

$$u\frac{\partial T}{\partial x} + v\frac{\partial T}{\partial y} = \alpha\left(\frac{\partial^2 T}{\partial x^2} + \frac{\partial^2 T}{\partial y^2}\right) \tag{4}$$

$$u\frac{\partial C}{\partial x} + v\frac{\partial C}{\partial y} = D\left(\frac{\partial^2 C}{\partial x^2} + \frac{\partial^2 C}{\partial y^2}\right) \tag{5}$$

where u, v, P, T and C are the volume-averaged velocity components, pressure, temperature and concentration, respectively. Note that C is the concentration of the constituent of interest, and that it signifies the number of kg of constituent per unit vol. of porous medium (fluid and solid). Properties μ and ρ are the solution viscosity and density, and K is the permeability of the porous medium. The thermal diffusivity α is defined as the thermal conductivity of the porous medium saturated with fluid, divided by the specific heat capacity of the fluid alone. The mass diffusivity D represents the diffusivity of the constitutent of interest measured through the fluid-saturated porous medium.

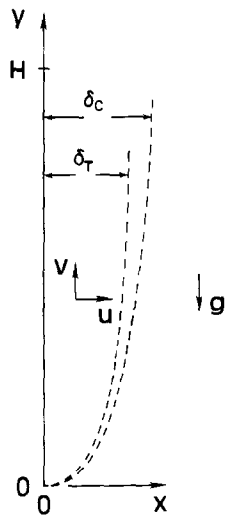

FIG. 1. Temperature and concentration boundary layers in natural convection near a vertical surface in a fluid-saturated porous medium.

Eliminating the pressure terms by cross-differentiating equations (2) and (3),

$$\frac{\partial u}{\partial y} - \frac{\partial v}{\partial x} = \frac{Kg}{\mu}\frac{\partial \rho}{\partial x} \tag{6}$$

and recognizing that at constant pressure the density depends on both temperature and concentration [1, 2], the Boussinesq-approximated momentum equation reduces to

$$\frac{\partial u}{\partial y} - \frac{\partial v}{\partial x} = -\frac{gK}{\nu}\left(\beta\frac{\partial T}{\partial x} + \beta_C\frac{\partial C}{\partial x}\right). \tag{7}$$

In this form β and β_C are the thermal expansion and concentration expansion coefficients

$$\beta = -\frac{1}{\rho}\left(\frac{\partial \rho}{\partial T}\right)_P, \quad \beta_C = -\frac{1}{\rho}\left(\frac{\partial \rho}{\partial C}\right)_P. \tag{8}$$

Finally, we focus on the boundary-layer regime where the temperature and concentration gradients are steep in a vertical slender region situated near the wall. Thus we work with the boundary-layer-approximated form of the momentum, energy and constituent conservation equations (the domain of applicability of this approximation is discussed in section 5):

$$\frac{\partial v}{\partial x} = \frac{gK}{\nu}\left(\beta\frac{\partial T}{\partial x} + \beta_C\frac{\partial C}{\partial x}\right) \tag{9}$$

$$u\frac{\partial T}{\partial x}+v\frac{\partial T}{\partial y}=\alpha\frac{\partial^2 T}{\partial x^2} \tag{10}$$

$$u\frac{\partial C}{\partial x}+v\frac{\partial C}{\partial y}=D\frac{\partial^2 C}{\partial x^2}. \tag{11}$$

The boundary conditions that apply on the two sides of the velocity, temperature and concentration boundary layers are

$$u=0,\quad T=T_0,\quad C=C_0\quad \text{at}\quad x=0 \tag{12}$$

and

$$v\to 0,\quad T\to T_\infty,\quad C\to C_\infty\quad \text{as}\quad x\to\infty. \tag{13}$$

In the next section we solve this boundary-layer heat and mass transfer problem based on scale analysis, leaving the more accurate results of similarity analysis for presentation in section 4.

3. SCALE ANALYSIS

The scales of the flow, temperature and concentration fields near the vertical surface of Fig. 1 can be determined based on order-of-magnitude analysis. Consider for this purpose the concentration boundary layer of height H and thickness δ_C, and the thermal boundary layer of height H and thickness δ_T. In general $\delta_C\neq\delta_T$; however, in order to illustrate the discussion that follows equation (25) later in this section, the concentration layer was drawn thicker than the thermal layer on Fig. 1.

Integrating equation (9) across the boundary layers, and invoking the reservoir conditions (13) yields

$$v=\frac{gK}{\nu}[\beta(T-T_\infty)+\beta_C(C-C_\infty)]. \tag{14}$$

This equation shows that the vertical boundary-layer flow is driven either by heat transfer ($|\beta\Delta T|\gg|\beta_C\Delta C|$), or by mass transfer ($|\beta_C\Delta C|\gg|\beta\Delta T|$), or by a combination of heat and mass transfer effects. In the scale analysis presented below we focus on the first two possibilities, saving the third for the similarity solution reported in section 4.

Heat-transfer-driven flow

In the limit where the buoyancy effect due to side heating is dominant,

$$|\beta\Delta T|\gg|\beta_C\Delta C| \tag{15}$$

the vertical velocity scale is, from equation (14),

$$v\sim\frac{gK}{\nu}\beta\Delta T. \tag{16}$$

In the thermal boundary layer (H, δ_T) the energy equation (10) indicates a balance between thermal diffusion from the side and vertical enthalpy flow,

$$u\frac{\Delta T}{\delta_T},\quad \text{or}\quad v\frac{\Delta T}{H}\sim\alpha\frac{\Delta T}{\delta_T^2}. \tag{17}$$

Since the principle of mass conservation (1) in the (H, δ_T) layer requires

$$\frac{u}{\delta_T}\sim\frac{v}{H}, \tag{18}$$

we conclude that the two convection scales in equation (17) are of the same order of magnitude; hence, energy conservation in the thermal boundary layer requires

$$v\frac{\Delta T}{H}\sim\alpha\frac{\Delta T}{\delta_T^2} \tag{19}$$

or

$$\delta_T\sim H\,Ra^{-1/2}, \tag{20}$$

where Ra is the Darcy-modified Rayleigh number used routinely in the field of natural convection heat transfer through porous media,

$$Ra=\frac{KgH\beta\Delta T}{\alpha\nu}. \tag{21}$$

The overall Nusselt number

$$Nu=\frac{q'}{k\Delta T} \tag{22}$$

scales as

$$Nu\sim\left(kH\frac{\Delta T}{\delta_T}\right)\Big/k\Delta T\sim Ra^{1/2}. \tag{23}$$

The fluid flow and heat transfer scales listed as equations (16), (20) and (23) agree within a factor of order one with the similarity solution reported for the pure heat transfer problem by Cheng and Minkowycz [8]. The new feature in the present problem is the mass transfer effected by the thermally driven vertical layer of scales (v, δ_T) determined above. In dimensionless form, the mass transfer rate can be expressed as an overall Sherwood number

$$Sh=\frac{j'}{D\Delta C} \tag{24}$$

or, in terms of the unknown concentration boundary-layer thickness δ_C,

$$Sh\sim\left(DH\frac{\Delta C}{\delta_C}\right)\Big/D\Delta C\sim\frac{H}{\delta_C}. \tag{25}$$

Thus the ability to estimate the mass transfer scale reduces to being able to estimate the concentration layer thickness δ_C.

The scale of δ_C depends on the relative size of δ_C and δ_T (Fig. 2). Integrating the constituent conservation equation (11) from the wall into the reservoir, we obtain

$$\frac{\mathrm{d}}{\mathrm{d}y}\int_0^{x>\max(\delta_T,\delta_C)}v(C-C_\infty)\,\mathrm{d}x=-D\left(\frac{\partial C}{\partial x}\right)_{x=0} \tag{26}$$

which states that the lateral diffusion of constituent into the vertical boundary-layer flow equals the rate of increase in the amount of constituent swept upward by the flow. The scaling equivalence recommended by

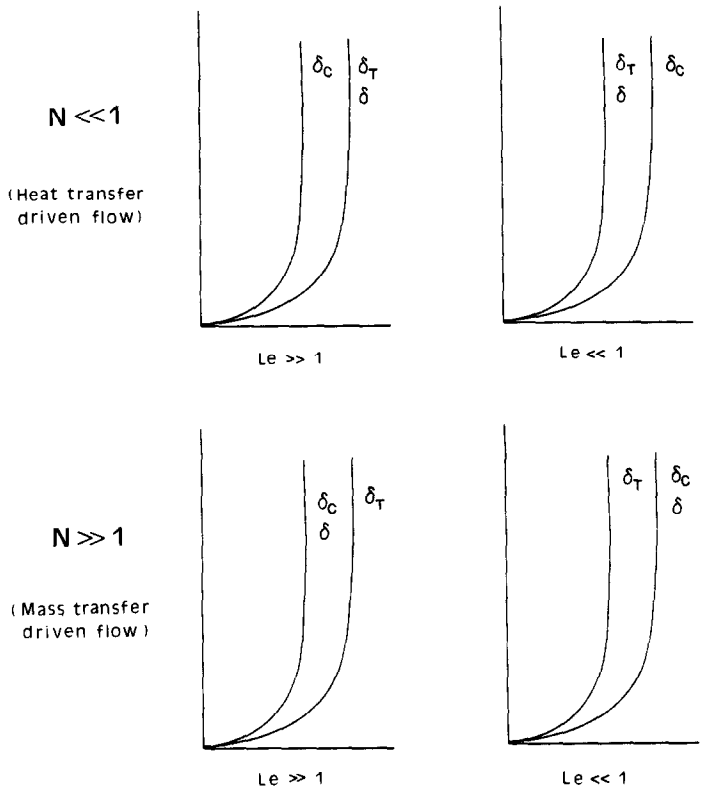

FIG. 2. The four limiting regimes in which the phenomenon of natural convection heat and mass transfer can exist.

equation (26) is

$$\frac{v\Delta C}{H}\min(\delta_T, \delta_C) \sim D\frac{\Delta C}{\delta_C}. \tag{27}$$

Note that the factor $\min(\delta_T, \delta_C)$ appearing on the LHS of the above equation is the transversal length scale of the upward flow of constituent. The effective thickness of this stream can be determined by recognizing that it must contain fluid that moves upward and, at the same time, it must contain constituent-rich fluid. In other words, the upward constituent stream must exist at the same time inside the velocity boundary layer (which in heat-transfer-driven flows is δ_T thick), and inside the δ_C-thick concentration boundary layer. Therefore, the constituent stream assumes as thickness the smaller of δ_T and δ_C: this is the choice made in equation (27) and used consistently throughout the scale analysis part of this study. As shown in section 5, this choice is validated by considerably more rigorous results obtained based on a similarity formulation of the same problem. It is easy to show that if one opts for the other choice in equation (27), i.e. if one replaces $\min(\delta_T, \delta_C)$ with $\max(\delta_T, \delta_C)$, the results of scale analysis are no longer in agreement with the trends exhibited by similarity solutions.

In conclusion, in order to determine the concentration boundary-layer thickness scale δ_C from equation (27) we must consider separately two possibilities, $\delta_C < \delta_T$ and $\delta_T < \delta_C$.

(a) $\delta_C \ll \delta_T$. Writing $v\Delta C\delta_C/H$ on the LHS of equation (27), and using the v scale given by equations (19) and (20) we obtain

$$\delta_C \sim H\,Ra^{-1/2}Le^{-1/2} \tag{28}$$

and

$$Sh \sim Ra^{1/2}Le^{1/2} \tag{29}$$

where Le is the Lewis number of the homogeneous porous medium, $Le = \alpha/D$. The condition necessary for the validity of the mass transfer scales (28) and (29) follows from writing one more time $\delta_C \ll \delta_T$, hence

$$Le \gg 1. \tag{30}$$

(b) $\delta_T \ll \delta_C$. In the opposite extreme, we write $v\Delta C\delta_T/H$ on the LHS of equation (27) and, in combination with equations (19) and (20), we obtain

$$\delta_C \sim H\,Ra^{-1/2}Le^{-1} \tag{31}$$

and

$$Sh \sim Ra^{1/2}Le. \tag{32}$$

These scales are valid if $\delta_T \ll \delta_C$, which means

$$Le \ll 1.$$

Mass-transfer-driven flow

The class of flows dominated by the buoyancy effect associated with mass transfer from the side can be

analyzed by setting

$$|\beta_C \Delta C| \gg |\beta \Delta T| \tag{33}$$

in the boundary-layer momentum equation (14), hence

$$v \sim \frac{gK}{\nu} \beta_C \Delta C. \tag{34}$$

This new velocity scale can be combined with the equivalence of scales demanded by the conservation of constituent in the concentration boundary layer (H, δ_C) (note that the velocity profile is δ_C thick in mass-transfer-driven flows)

$$\frac{v \Delta C}{H} \delta_C \sim D \frac{\Delta C}{\delta_C} \tag{35}$$

The resulting mass transfer scales of flows driven by buoyancy due to concentration nonuniformity are

$$\delta_C \sim H(Ra\, Le\, |N|)^{-1/2} \tag{36}$$

and

$$Sh \sim (Ra\, Le\, |N|)^{1/2} \tag{37}$$

where the 'buoyancy ratio' [1]

$$N = \frac{\beta_C \Delta C}{\beta \Delta T} \tag{38}$$

has an absolute value greater than 0(1). Note that the scale analysis of mass-transfer-driven flows is valid for both positive and negative values of N, provided the absolute value of N is much larger than one. The only change that occurs when N is negative and large in absolute value is that the double boundary layers sketched in Figs. 1 and 2 develop in the negative y direction, since the flow will then be downward. The scale analysis does not hold when N is comparable with -1: in that range the temperature and concentration buoyancy effects are of the same order of magnitude and in opposite directions, hence the δ_T layer tends to start from one end of the wall while the δ_C layer tends to start from the other. If it exists, the resulting flow does not have the parallel double boundary-layer structure (with the same starting point) assumed both in the analysis and in the similarity solutions of section 4. This is probably the reason why similarity solutions of the type sketched in Figs. 1 and 2 were not found in the range $-1 < N < 0$ when $Le = 1$ (see section 4).

In order to determine the heat transfer scales, we first integrate the boundary-layer energy equation (10)

$$\frac{d}{dy} \int_0^{x \gg \max(\delta_T, \delta_C)} v(T - T_\infty)\, dx = -\alpha \left(\frac{\partial T}{\partial x} \right)_{x=0} \tag{39}$$

Next, we recognize that the vertical enthalpy contains fluid moving upward and, at the same time, fluid that has been heated by the wall. The moving stream is δ_C thick in mass-transfer-driven flows, Fig. 2, while the heated layer is δ_T thick. In conclusion, the enthalpy stream must fit the inside both δ_C and δ_T layers, hence its transversal dimension is $\min(\delta_T, \delta_C)$. The equivalence of scales recommended by equation (39) is therefore

$$\frac{v \Delta T}{H} \min(\delta_T, \delta_C) \sim \alpha \frac{\Delta T}{\delta_T}. \tag{40}$$

In what follows we discuss separately the two possibilities $\delta_T \ll \delta_C$ and $\delta_C \ll \delta_T$.

(c) $\delta_T \ll \delta_C$. Substituting $v \Delta T \delta_T / H$ on the LHS of equation (40), and relying on the v scale given by equations (35) and (36) yields

$$\delta_T \sim H(Ra\, |N|)^{-1/2} \tag{41}$$

and

$$Nu \sim (Ra\, |N|)^{1/2}. \tag{42}$$

These heat transfer scales are valid provided $\delta_T \ll \delta_C$, in other words if

$$Le \ll 1. \tag{43}$$

(d) $\delta_C \ll \delta_T$. In the opposite extreme, we use $v \Delta T \delta_C / H$ in equation (40), and the resulting heat transfer scales are

$$\delta_T \sim H\, Le^{1/2} (Ra\, |N|)^{-1/2} \tag{44}$$

and

$$Nu \sim Le^{-1/2} (Ra |N|)^{1/2}. \tag{45}$$

The condition for scales (44) and (45) to be valid is $\delta_C \ll \delta_T$, which translates into

$$Le \gg 1. \tag{46}$$

The main conclusions of the scale analysis presented in this section are summarized in Table 1 and Fig. 2. In

Table 1. Flow, heat and mass transfer scales near a vertical wall in a porous medium with combined buoyancy effects

Driving mechanism	v	Nu	Sh	Observations
Heat transfer	$\frac{\alpha}{H} Ra$	$Ra^{1/2}$	$(Ra\, Le)^{1/2}$	$Le \gg 1$
$\|N\| \ll 1$	$\frac{\alpha}{H} Ra$	$Ra^{1/2}$	$Ra^{1/2} Le$	$Le \ll 1$
Mass transfer	$\frac{\alpha}{H} Ra\|N\|$	$(Ra\|N\|)^{1/2}$	$(Ra\, Le\|N\|)^{1/2}$	$Le \ll 1$
$\|N\| \gg 1$	$\frac{\alpha}{H} Ra\|N\|$	$Le^{-1/2}(Ra\|N\|)^{1/2}$	$(Ra\, Le\|N\|)^{1/2}$	$Le \gg 1$

the next section we report a series of similarity solutions that validate the results of scale analysis for $|N| \ll 1$ and $|N| \gg 1$, and focus more closely on the intermediate regime $|N| \sim 1$.

4. SIMILARITY SOLUTIONS

The number of horizontal entries in Table 1 shows that we have a maximum of four transversal length scales on which we could base the nondimensionalization of the problem statement formulated in section 2. Out of these, the most sensible choice is the thermal boundary-layer thickness for heat-transfer-driven flows ($N \ll 1$) because its scale is independent of Lewis number, and because similarity heat transfer solutions for $N = 0$ have already been reported by Cheng and Minkowycz [8]. Therefore, we introduce the dimensionless similarity profiles for vertical velocity, $f'(\eta)$; temperature, $\theta(\eta)$; and concentration $c(\eta)$,

$$v = -\frac{\alpha}{y} Ra_y f'(\eta) \tag{47}$$

$$u = \frac{\alpha}{2y} Ra_y^{1/2}(f - \eta f') \tag{48}$$

$$\theta(\eta) = \frac{T - T_\infty}{T_0 - T_\infty} \tag{49}$$

$$c(\eta) = \frac{C - C_\infty}{C_0 - C_\infty} \tag{50}$$

where

$$\eta = \frac{x}{y Ra_y^{-1/2}} \tag{51}$$

and

$$Ra_y = \frac{g\beta K y(T_0 - T_\infty)}{\alpha\nu}. \tag{52}$$

And, using the streamfunction formulation ($u = \partial\psi/\partial y$, $v = -\partial\psi/\partial x$),

$$\psi = \alpha Ra_y^{1/2} f(\eta) \tag{53}$$

the governing equations reduce to

$$f'' = -\theta' - Nc' \tag{54}$$

$$\theta'' = \frac{1}{2} f\theta' \tag{55}$$

$$c'' = \frac{1}{2} fc' Le \tag{56}$$

subject to six boundary conditions

$$f = 0, \quad \theta = 1, \quad c = 1 \quad \text{at} \quad \eta = 0 \tag{57}$$

and

$$f' \to 0, \quad \theta \to 0, \quad c = 0 \quad \text{as} \quad \eta \to \infty. \tag{58}$$

The problem stated as equations (54)–(58) was solved numerically for a discrete sequence of (N, Le) pairs. The numerical procedure was the standard 'shooting'

Table 2. Summary of similarity solutions for local Nusselt and Sherwood numbers

N	Le	$Nu_y Ra_y^{-1/2}$	$Sh_y Ra_y^{-1/2}$
4	1	0.992	0.992
	2	0.899	1.431
	4	0.798	2.055
	6	0.742	2.533
	8	0.707	2.936
	10	0.681	3.290
	100	0.521	10.521
3	1	0.888	0.888
	2	0.810	1.286
	4	0.728	1.852
	6	0.683	2.286
	8	0.655	2.652
	10	0.634	2.973
	100	0.506	9.532
2	1	0.769	0.769
	2	0.710	1.122
	4	0.650	1.624
	6	0.618	2.009
	8	0.597	2.332
	10	0.582	2.617
	100	0.490	8.424
1	1	0.628	0.628
	2	0.593	0.930
	4	0.559	1.358
	6	0.541	1.685
	8	0.529	1.960
	10	0.521	2.202
	100	0.470	7.139
0.8	1	0.595	0.595
0.5	1	0.543	0.543
0.2	1	0.486	0.486
0.1	1	0.465	0.465
0	1	0.444	0.444
	2	0.444	0.683
	4	0.444	1.019
	6	0.444	1.275
	8	0.444	1.491
	10	0.444	1.680
	100	0.444	5.544
-1		no flow	no flow
-1.1	1	0.144	0.144
-1.2	1	0.199	0.199
-1.5	1	0.314	0.314
-1.9	1	0.421	0.421
-2.0	1	0.444	0.444
-3.0	1	0.628	0.628
	2	0.488	0.832
-4.0	1	0.769	0.769
	2	0.627	1.046
-5.0	1	0.888	0.888
	2	0.739	1.220

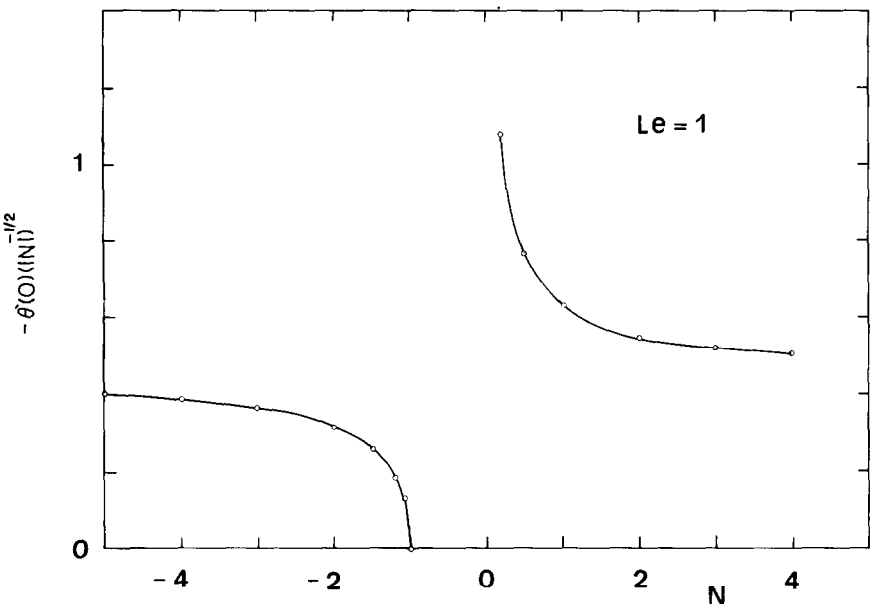

FIG. 3. The effect of buoyancy ratio N on the local Nusselt number, equation (61), when $Le = 1$.

method, by which equations (54)–(56) were integrated from $\eta = 0$ onward using the fourth-order Runge–Kutta method. To initiate the integration it was necessary to guess the values of $f'(0)$, $\theta'(0)$ and $c'(0)$ and to adjust these guesses until the outer boundary conditions (58) were satisfied. The numerical results listed in Table 2 were all obtained based on the shooting success criterion

$$\max [f'(\eta), \theta(\eta), c(\eta)] \leqslant 2 \times 10^{-4}. \tag{59}$$

A shooting distance $\eta \geqslant 15$ was found to be adequate in simulating the $\eta \to \infty$ limit of equations (58). The required shooting distance depended primarily on the Lewis number, as illustrated in Figs. 4a and 6. The $\Delta\eta$ step used in performing the calculations summarized in Table 2 was $\Delta\eta = 0.0025$; this step size was found to be small enough to render the numerical values listed in Table 2 insensitive to further decreases in $\Delta\eta$. It is worth pointing out that in the case of negative values of the buoyancy ratio N, the similarity momentum equation (54) was replaced by

$$f'' = \theta' + Nc', \tag{60}$$

in order to account for the occurrence of flow in the negative y direction when the opposing effect of concentration buoyancy overwhelms the flow tendency sketched in Fig. 1.

Relevant to the numerical verification of the scaling results of section 3 is the fact that the $[\theta'(0), c'(0)]$ values listed in Table 2 are related to the local Nusselt and Sherwood numbers,

$$Nu_y = -\theta'(0)\, Ra_y^{1/2} \tag{61}$$

and

$$Sh_y = -c'(0)\, Ra_y^{1/2}. \tag{62}$$

These local values should agree within a numerical factor of order one with the overall scales summarized in Table 1, provided $|N|$ is not comparable with 0(1). We compared the similarity results of this section with the scaling results of section 3 by focusing individually on the two effects that influence the heat and mass transfer phenomenon, namely, the effect of buoyancy ratio (Figs. 3 and 4) and the effect of Lewis number (Figs. 5 and 6).

The effect of buoyancy ratio

Figures 3 and 4 show how the thermal and concentration boundary layers react to changes in the buoyancy ratio N, while the Lewis number is being held fixed ($Le = 1$). Note that in this test the thermal and concentration boundary layers are of equal thickness. According to Table 1 and equations (61) and (62), the values of $-\theta'(0)$ and $-c'(0)$ should both be proportional to $(|N|)^{1/2}$ as the absolute value of the buoyancy ratio becomes greater than one. This trend is confirmed by the data assembled in Fig. 3, which show that the similarity solutions for $-\theta'(0)/(|N|)^{1/2}$ and $-c'(0)/(|N|)^{1/2}$ approach a constant in the vicinity of 0.45 as $|N|$ becomes much greater than one. Note also that the $0 < N < 1$ data of Fig. 3 support the scaling results listed in the upper row of Table 1: both $-\theta'(0)$ and $-c'(0)$ approach a constant in the vicinity of 0.45 as N approaches zero. In fact, Table 2 shows that this limiting constant is

$$\lim_{\substack{N \to 0 \\ Le = 1}} [\theta'(0), c'(0)] = -0.444, \tag{63}$$

which agrees with the earlier calculations of Cheng and

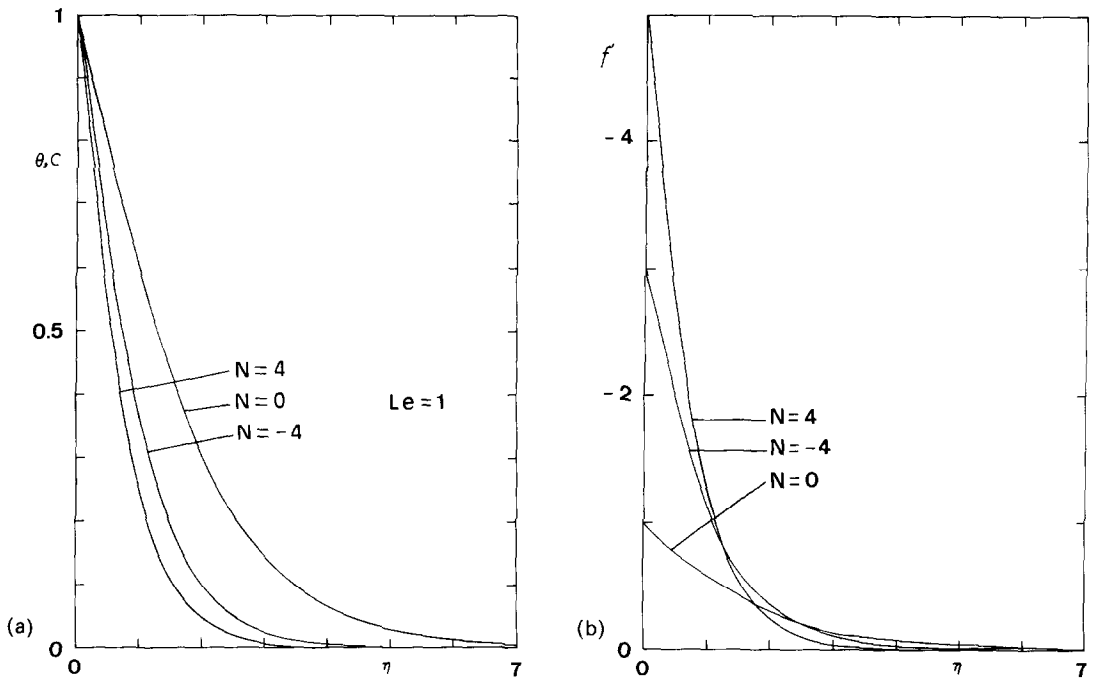

FIG. 4. The effect of buoyancy ratio N when $Le = 1$: (a) temperature or concentration profiles; (b) velocity profiles.

Minkowycz [8] for local Nusselt number in the absence of buoyancy due to concentration gradients.

Finally, Fig. 3 shows that for $Le = 1$ no similarity solutions were found in the range $-1 < N < 0$ where the two buoyancy effects are of the same order of magnitude and in opposite directions. When $N = -1$, the two buoyancy effects cancel each other and the solution is one of 'no flow'. This conclusion can also be reached analytically by plugging $Le = 1$ and $N = -1$ in the boundary-layer momentum equation (14), which can be rewritten as

$$v = \frac{gK\beta\Delta T}{\nu}(\theta + Nc). \tag{64}$$

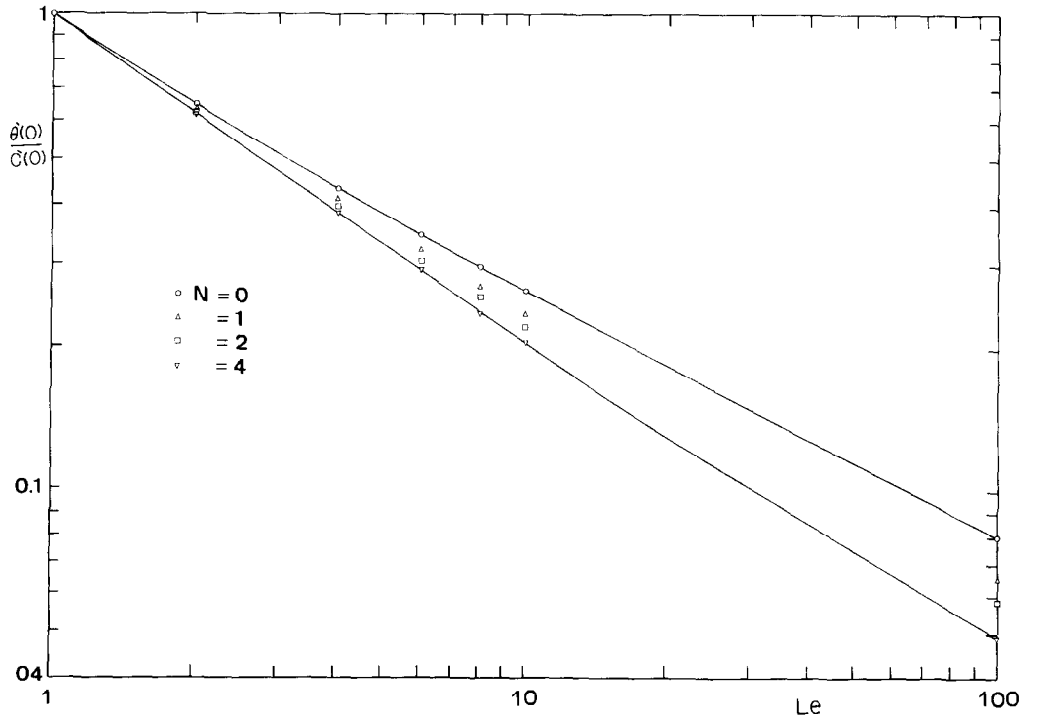

FIG. 5. The effect of Lewis number on the ratio of local heat transfer rate divided by the local mass transfer rate.

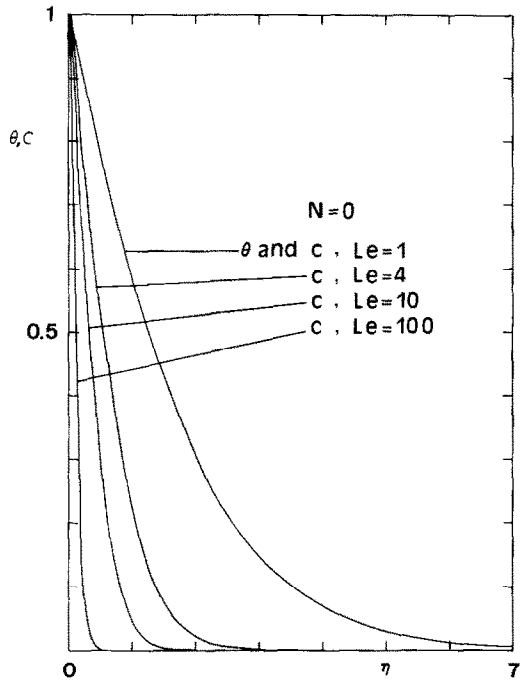

FIG. 6. The effect of Lewis number on the concentration profile in heat-transfer-driven flows ($N = 0$).

Since at $Le = 1$ the θ and c profiles are identical, the value $N = -1$ renders the RHS of equation (64) zero, hence $v = 0$ and the 'no-flow' conclusion listed in Table 2. The absence of similarity solutions in the range $-1 < N < 0$ when $Le = 1$, may be related to the absence of the parallel boundary-layer structure (Fig. 1) assumed as basis for the similarity solution formulation. This observation is discussed further immediately below equation (38).

The effect of Lewis number

According to the top line in Table 1, in heat-transfer-driven boundary layers in porous media with large Lewis numbers, the ratio Nu/Sh must be of the same order as $Le^{-1/2}$. This trend is confirmed by the $N = 0$ similarity solution results plotted in Fig. 5: the ratio Nu_y/Sh_y parallels the $Le^{-1/2}$ line very closely as Le increases from 1 to 100. Figure 6 shows the corresponding response of the concentration profile as Le increases: the concentration boundary layer shrinks relative to the thermal layer, as the ratio δ_C/δ_T scales as $Le^{-1/2}$.

Figure 5 shows also that as the buoyancy ratio N increases above 0(1), the ratio Nu_y/Sh_y shows an increasingly steeper dependence on Lewis number. This behavior is consistent with the results of scale analysis: the last line in Table 1 indicates that as $|N|$ becomes very large, the ratio Nu/Sh should vary as Le^{-1}.

Finally, it is interesting to follow the $N = 0$ data from right to left in Fig. 5 and to notice that the slope of the Nu_y/Sh_y vs Le curve increases gradually as Le approaches 0(1). The steepening of the curve is again consistent with the scaling shown for $|N| \ll 1$ and $Le \ll 1$ in Table 1: according to the second line in that table, the ratio Nu/Sh must scale as Le^{-1} at Lewis numbers smaller than 0(1).

5. SUMMARY

In this study we relied on pure scaling arguments to show that the phenomenon of natural convection heat and mass transfer near a vertical surface in a porous medium conforms to one of four possible regimes, depending on the buoyancy ratio $|N|$ and the Lewis number Le (Table 1). Similarity solutions for this multiple scale boundary-layer problem (Table 2) confirmed the validity of the order-of-magnitude estimates produced by scale analysis.

The scale and similarity analyses are both based on the boundary-layer approximation of the complete governing equations [compare equation (1)–(5) with equations (9)–11)]. Therefore, the results reported in this study are valid provided the concentration and temperature boundary layers are slender,

$$(\delta_C, \delta_T) \ll H \tag{65}$$

Recalling that $Nu \sim H/\delta_T$ and $Sh \sim H/\delta_C$, the validity criterion (65) translates into the condition that the Nu and Sh scales of the four regimes summarized in Table 1 must all be greater than 0(1) to be valid.

Finally, an observation made necessary by the commentary provided by an anonymous reviewer of this manuscript: 'scale analysis' is a self-standing method of solution in the field of convection; that is, it is an analytical method that is capable of yielding useful results in the same manner that another method might be capable of yielding a solution to the same problem. However, just like any other method, the method of scale analysis has its own rules [9], and it is this set of rules that distinguishes it from the more classical analytical methods.

Acknowledgement—This research was sponsored by the National Science Foundation through Grant No. MEA-82-07779.

REFERENCES

1. S. Ostrach, Natural convection with combined driving forces, *PhysicoChemical Hydrodynamics* **1**, 233–247 (1980).
2. P. Cheng, Heat transfer in geothermal systems, *Adv. Heat Transfer* **14**, 1–105 (1979).
3. D. A. Nield, Onset of thermohaline convection in a porous medium, *Water Resources Res.* **4**, 553–560 (1968).
4. G. Z. Gershuni, E. M. Zhukhovitskii and D. V. Lyubimov, Thermal concentration instability of a mixture in a porous medium, *Soviet Phys. Dokl.* **21**, 375–377 (1976).
5. J. S. Turner and L. B. Gustafson, The flow of hot saline solutions from vents in the sea floor—some implications for exhalative massive sulfide and other ore deposits, *Econ. Geol.* **73**, 1082–1100 (1978).
6. A. A. Khan and A. Zebib, Double diffusive instability in a vertical layer of a porous medium, *J. Heat Transfer* **103**, 179–181 (1981).

7. A. Raptis, G. Tzivanidis and N. Kafousias, Free convection and mass transfer flow through a porous medium bounded by an infinite vertical limiting surface with constant suction, *Lett. Heat Mass Transfer* **8**, 417–424 (1981).
8. P. Cheng and W. J. Minkowycz, Free convection about a vertical flat plate embedded in a saturated porous medium with application to heat transfer from a dike, *J. Geophys. Res.* **82**, 2040–2044 (1977).
9. A. Bejan, *Convection Heat Transfer*, Chap. 1. Wiley, New York, (1984).

TRANSFERT DE CHALEUR ET DE MASSE PAR CONVECTION NATURELLE DANS UN MILIEU POREUX

Résumé—On rapporte une étude fondamentale de la convection naturelle de chaleur et de masse près d'une surface verticale noyée dans un milieu poreux saturé de fluide. L'effet de pesanteur est dû à la variation de température et de concentration à travers la couche limite. Dans la première partie de l'étude, l'analyse d'échelle montre que la convection naturelle se fait selon l'un des quatre régimes possibles, selon les valeurs du rapport de pesanteur N et du nombre de Lewis Le. Les échelles des flux transférés de chaleur et de masse sont déterminées pour chaque régime. Dans la seconde partie de l'étude, le problème de couche limite est résolu à travers une formulation de similitude dans les domaines $-5 < N < 4$ et $1 < Le < 100$. Les solutions de similitude confirment la validité de l'ordre de grandeur limitant les résultats révélés par l'analyse d'échelle.

WÄRME- UND STOFFTRANSPORT INFOLGE NATÜRLICHER KONVEKTION IN EINEM PORÖSEN MEDIUM

Zusammenfassung—Diese Arbeit berichtet von einer grundlegenden Untersuchung des Phänomens des Wärme- und Stofftransports infolge natürlicher Konvektion an einer senkrechten Wand in einem fluidgesättigten, porösen Medium. Der Auftriebseffekt entsteht infolge der Unterschiede von Temperatur und Konzentration innerhalb der Grenzschicht. Die Untersuchung gliedert sich in zwei Teile. Im ersten Teil zeigt eine Abschätzung der Größenordnungen, daß die Erscheinungsweise der natürlichen Konvektion in vier mögliche Bereiche eingeteilt werden kann, was vom Auftriebsverhältnis N und der Lewis-Zahl Le abhängt. Die Größenordnung von Wärme- und Stofftransportraten wurde für jede Erscheinungsform ermittelt. Im zweiten Teil der Untersuchung wird das Grenzschichtproblem mit Hilfe einer Ähnlichkeitstransformation für Auftriebsverhältnisse $-5 \leqslant N \leqslant 4$ und Lewis-Zahlen $1 \leqslant Le \leqslant 100$ gelöst. Die Ähnlichkeitslösungen bestätigen die Gültigkeit der Abschätzung der Größenordnung.

ЕСТЕСТВЕННОКОНВЕКТИВНЫЙ ТЕПЛОМАССОПЕРЕНОС В ПОРИСТОЙ СРЕДЕ

Аннотация—Настоящая работа посвящена исследованию основных закономерностей естественноконвективного тепломассопереноса у вертикальной поверхности, погруженной в насыщенную жидкостью пористую среду. Подъемный эффект обусловлен изменением температуры и концентрации поперек пограничного слоя. Работа состоит из двух частей. В первой части с помощью анализа масштабов показано, что в зависимости от значений безразмерной подъемной силы N и числа Льюиса Le могут существовать четыре режима естественной конвекции. Для каждого из режимов определены интенсивности тепломассопереноса. Вторая часть работы посвящена решению задачи о пограничном слое методами теории подобия в диапазонах коэффициента подъемной силы $-5 \leq N \leq 4$ и числа Льюиса $1 \leq Le \leq 100$. Автомодельные решения подтверждают по порядку величины справедливость предельных оценок, найденных анализом размерностей.